Fabrication of Polymer/Selective-Flake Nanocomposite Membranes and Their Use in Gas Separation

Hae-Kwon Jeong,[†,⊥] Wojtek Krych,[‡,⊥] Harikrishnan Ramanan,[§] Sankar Nair,[∥] Eva Marand,*[,‡] and Michael Tsapatsis*[,†,§]

Department of Chemical Engineering and Materials Science, University of Minnesota, Minneapolis, Minnesota 55108, Department of Chemical Engineering, Virginia Polytechnic Institute and State University, Blacksburg, Virginia 24601, Department of Chemical Engineering, University of Massachusetts, Amherst, Massachusetts 01002, and School of Chemical Engineering & Biomolecular Engineering, Georgia Institute of Technology, Atlanta, Georgia 30332

Received May 27, 2004

Here, we report for the first time the fabrication of polymer/selective-flake nanocomposite membranes which can, in principle, be scaled down to submicrometer structures. A layered aluminophosphate with a porous net layer is used as a selective phase and a polyimide as a continuous phase. The microstructures of the nanocomposite membranes are investigated using various characterization techniques including X-ray diffraction, NMR, transmission electron microscopy, small-angle neutron scattering, and dynamic mechanical thermal analysis. Nanocomposite membranes with 10 wt % layered aluminophosphate show substantial enhancement in performance with oxygen selectivity over nitrogen as high as 8.9 (as compared to 3.6 for pure polymer) and carbon dioxide selectivity over methane as high as 40.9 (as compared to 13.4 for pure polymer) in room-temperature permeation measurements. This improved performance, along with permeability estimation through the aluminophosphate layers with a semiempirical model, suggests that the layered aluminophosphate plays a role as a molecular sieve favoring smaller molecules.

Introduction

Gas separations by membranes are currently dominated by polymeric materials that can be produced as hollow fibers with thin (100 nm) permselective skins.[1] However, despite the ability to produce robust membranes at relatively low cost, wider implementation of this technology is hindered by intrinsic permeability and selectivity limitations of the polymeric materials it currently employs. Composites of polymers with microporous materials such as carbons, zeolites, and other molecular sieve oxides were proposed as new membrane materials.[2−10] It has been argued that these mixed-matrix materials may retain polymer processability while improving permselective properties due to the superior ability for molecular recognition by the microporous component. However, a large amount of microporous phase is required to obtain substantial enhancement of permselective properties, leading to compromised mechanical properties and processing difficulties. Moreover, since all of the microporous additives used so far have particle sizes larger than approximately 100 nm, the obtained microstructures, in principle, cannot be easily scaled down to submicrometer thick films. Here, we report the synthesis of a polyimide/selective-aluminophosphate-flake (hereafter, PSF) nanocomposite that shows promising performance for gas separation applications with a small amount of added aluminophophate and a microstructure that can, in principle, be scaled down to 100 nm films.

The concept of selective flakes is an extension of the concept of impermeable layers.[11] Regarding the latter, it is well established that incorporation of small amounts of appropriately oriented impermeable layers in polymer composites can lead to considerable reduction of permeability and improvement of thermal and mechanical stability.[12,13] Commercially available polymer-layered silicate (PLS) nanocomposites with improved barrier

* Correspondence for polymer synthesis and permeation measurement should be addressed to E.M. E-mail: emarand@vt.edu. Correspondence for AlPO synthesis, microstructural characterization, and analysis of results should be addressed to M.T. E-mail: tsapatsi@cems.umn.edu.

[†] University of Minnesota.

[‡] Virginia Polytechnic Institute and State University.

[§] University of Massachusetts.

[∥] Georgia Institute of Technology.

[⊥] These authors contributed equally to this work.

(1) Baker, R. W. *Ind. Eng. Chem. Res.* **2002**, *41*, 1393−1411.

(2) Zimmerman, C. M.; Singh, A.; Koros, W. J. *J. Membr. Sci.* **1997**, *137*, 145−154.

(3) Mahajan, R.; Koros, W. J. *Ind. Eng. Chem. Res.* **2000**, *39*, 2692−2696.

(4) Pechar, T. W.; Tsapatsis, M.; Marand, E.; Davis, R. *Desalination* **2002**, *146*, 3−9.

(5) Cornelius, C. J.; Marand, E. *J. Membr. Sci.* **2002**, *202*, 97−118.

(6) Tantekin-Ersolmaz, S. B.; Atalay-Orala, C.; Tather, M.; Erdem-Senatalar, A.; Schoeman, B.; Sterte, J. *J. Membr. Sci.* **2000**, *175*, 285−288.

(7) Gur, T. M. *J. Membr. Sci.* **1994**, *93*, 283−289.

(8) Yong, H. H.; Park, N. C.; Kang, Y. S.; Won, J.; Kim, W. N. *J. Membr. Sci.* **2001**, *188*, 151−163.

(9) Chung, T. S.; Chan, S. S.; Wang, R.; Lu, Z. H.; He, C. B. *J. Membr. Sci.* **2003**, *211*, 91−99.

(10) Vu, D. Q.; Koros, W. J.; Miller, S. J. *J. Membr. Sci.* **2003**, *211*, 311−334.

(11) Cussler, E. L. *J. Membr. Sci.* **1990**, *52*, 275−288.

10.1021/cm049154u CCC: $27.50
Published on Web 09/09/2004

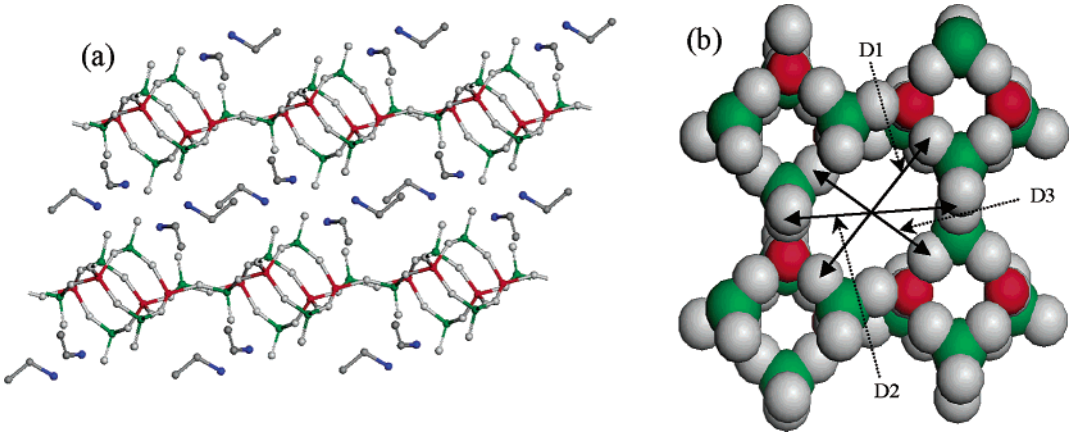

Figure 1. Crystal structure of a layered AlPO with 8MRs: (a) projection parallel to the layers, (b) projection perpendicular to the layers indicating the dimensions of the 8MR (oxygen center-to-center distances, D1 = 7.477 Å, D2 = 6.333 Å, D3 = 6.213 Å). The effective pore size is about 4.44 × 3.29 × 3.17 Å (after subtraction of the oxygen ionic radius from oxygen center-to-center distances). Red, green, and gray represent Al, P, and O atoms, respectively. Interlayer ethylammonium cations are shown as blue (nitrogen) and gray (carbon) dots.

properties are a testimony to the processing efficiency and potential for property improvement.[14−18] The extension to selective layers may lead to improvements in membrane technology similar to advances in coatings, device, and packaging technologies currently made by the use of PLS nanocomposites.

Experimental Section

Syntheses. A polyimide used as a continuous phase was synthesized according to the literature.[5,19,20] Polyimides are commercially available polymeric membrane materials for gas separation.[21] The polyimide employed in this study was 56100 MW (hexafluoroisopropylidene) dipthalic anhydride−(hexafluoroisopropylidene) 8% dianiline−diaminobenzoic acid (6FDA−6FpDA-8%−DABA) with a molecular weight distribution of 1.8. This polymer is soluble in tetrahydrofuran (THF) and has good mechanical, thermal, and transport properties.[5,20]

A layered aluminophosphate selected among several reported by Xu and co-workers[22] (hereafter, layered AlPO) having AlPO sheets with the 2-D net structure defined by four-, six-, and eight-membered rings (4MR, 6MR, and 8MR) (rings of interconnected AlO_4 and PO_4 tetrahedra) was used as the inorganic molecular sieve phase. The large opening in the AlPO 4 × 6 × 8 net is an 8MR with an estimated opening of ca. 4.44 × 3.28 × 3.17 Å (see Figure 1).[22] For layered AlPO synthesis, we followed the procedure of ref 22. In a typical layered AlPO synthesis, aluminum triisopropoxide (8.0 g) was added to the mixture of ethylene glycol (EG) (66.0 g) and 1-butanol (80.0 g). The mixture was stirred until homogeneous. Then ethylamine (34.72 g, 70 wt % in water) was added, and then phosphoric acid (13.44 g, 85 wt % in water) was added dropwise. The entire mixture was stirred until homogeneous, sealed in a Teflon-lined autoclave, filling about 70% of the volume, and heated to 180 °C for 13 days under autogenous pressure. Upon recovery from the mother liquor by vacuum filtration and after being washed with distilled water and dried at ambient temperature, the solid material was collected.

Fabrication of Nanocomposite Membranes. Before mixing with polymer, the layered AlPO was intercalated and swollen with a long-chain surfactant. This step is considered to be important for two reasons: (1) to make the material compatible with polymer and (2) to give room for the polymer chain to penetrate into the interlayer spacing of the layers. For the swelling procedure, 0.2 g of the as-synthesized aluminophosphate was well mixed in 40 g of aqueous cetyltrimethyammonium chloride (Sigma-Aldrich, 25 wt % in water).[23] Then 1.5 g of tetrapropylammonium hydroxide (Alpha Chemical, 40 wt % in water) was added. The ion exchange reaction was then carried out at elevated temperature (about 80 °C) for 16 h. The swollen AlPO was then washed with a copious amount of distilled water and filtered and dried at about 80 °C overnight. TGA analysis (not given here) confirmed that the ethylamine within the interlayer spacing, which holds the layers via hydrogen bonding, was partially replaced with the surfactant, composing about 30 wt % of the swollen AlPO.

The intercalated AlPO was then added in the predissolved polyimide in THF on the basis of the mass percentage of inorganic material desired. The mixture was allowed to mix for 4 days and then poured into 6.2 cm diameter Teflon pans, coating the bottom of the pan. Once cast, the pans were covered with glass, and a weight was placed on the glass to keep the THF from evaporating too quickly. After approximately 5−6 days, the membranes (∼100 μm thick) began to peel from the Teflon pans and were removed. The membranes were then annealed by heating them under vacuum at 323 K for 5 h, raising the temperature to 423 K for 5 h, and finally raising T to 493 K for 12 h.

Permeation Measurements. The gas permeation data obtained in this study are based on a time-lag method.[24] This method measures pressure increases in a constant downstream volume as a function of time to determine permeability. Each test was performed after the sample was degassed to a pressure of 1−10 mTorr and the system reached thermal equilibrium. This particular study focused on the single gas permeation measurements of He, O_2, N_2, CH_4, and CO_2, all at 99.999% purity. The temperature was 308 K and the feed pressure was 4 atm for all measurements. Each membrane was tested three times for each gas, and the average result

(12) Falla, W. R.; Mulski, M.; Cussler, E. L. *J. Membr. Sci.* **1996**, *119*, 129−138.
(13) Eitzman, D. M.; Melkote, R. R.; Cussler, E. L. *AIChE J.* **1996**, *42*, 2−9.
(14) Kornmann, X. *Division of Polymer Engineering*; Lulea University of Technology: Lulea, 2000.
(15) Kloprogge, J. T. *J. Porous Mater.* **1998**, *5*, 5−41.
(16) Giannelis, E. P. *Appl. Organomet. Chem.* **1998**, *12*, 675−680.
(17) Yano, K.; Usuki, A.; Okada, A. *J. Polym. Sci., Part A* **1997**, *35*, 2289−2294.
(18) Bharadwaj, R. K. *Macromolecules* **2001**, *34*, 9189−9192.
(19) Cornelius, C.; Hibshman, C.; Marand, E. *Sep. Purif. Technol.* **2001**, *25*, 181−193.
(20) Cornelius, C. J.; Marand, E. *Polymer* **2002**, *43*, 2385−2400.
(21) Sullivan, D. M.; Bruening, M. L. *Chem. Mater.* **2003**, *15*, 281−287.
(22) Gao, Q. M.; Li, B. Z.; Chen, J. S.; Li, S. G.; Xu, R. R.; Williams, I.; Zheng, J. Q.; Barber, D. *J. Solid State Chem.* **1997**, *129*, 37−44.
(23) Corma, A.; Fornes, V.; Pergher, S. B.; Maesen, T. L. M.; Buglass, J. G. *Nature* **1998**, *396*, 353−356.
(24) Pye, D. G.; Hoehn, H. H.; Panar, M. *J. Appl. Sci.* **1976**, *20*, 1921.

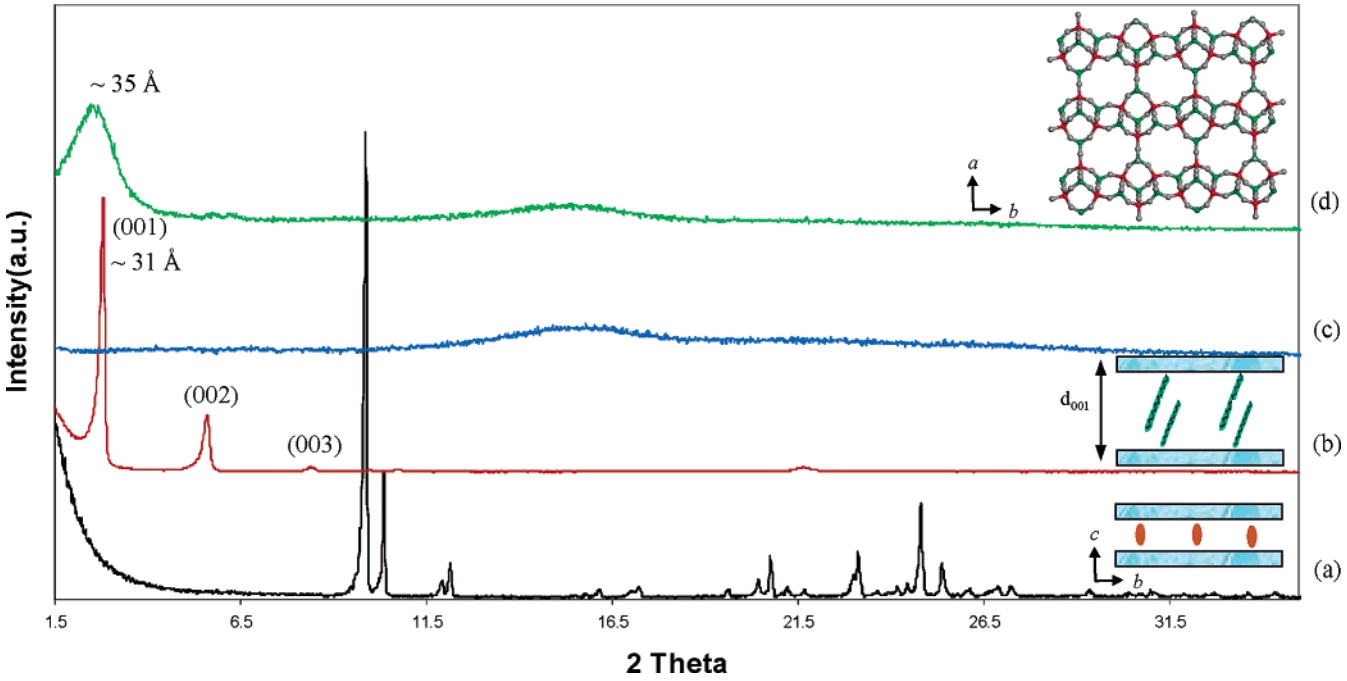

Figure 2. X-ray diffraction patterns of (a) as-synthesized layered AlPO, (b) swollen layered AlPO, (c) pure polyimide, and (d) a 10 wt % PSF nanocomposite. Expansion of the basal spacing (d_{001}) upon ion exchange is illustrated in the inset. The pore structure of the single layer of AlPO (top view) is illustrated in the inset.

was recorded. The percent error associated with the permeation measurement is about 5%.

Characterization. The XRD patterns were recorded with an X-ray diffractometer (Phillips X'pert) using Cu Kα radidation. The solid-state ^{27}Al and ^{31}P NMR spectra were obtained on a Bruker DSX300 with an MAS probe at room temperature. The chemical shift scales were externally set to zero for the ^{27}Al and ^{31}P signals of aqueous $Al_2(NO_3)_3$ and H_3PO_4 (85 wt %), respectively. The TEM images were collected on a JEOL JEM-2000FXII electron microscope operating at a voltage of 200 kV. Samples for TEM analysis are prepared by room-temperature microtomy. Pieces of the 10 wt % PSF nanocomposite membrane were transferred into curing molds, and a few drops of epoxy (low-temperature EXTEC curing resin) were poured over them. Samples were allowed to cure for 3−5 h at 45 °C. The surface revealing the cross-section of the membrane was microtomed using the Reichert ULTRACUT microtome equipped with a Diatome diamond knife (at room-temperature conditions, 25 °C) to get ultrathin sections (~600−1000 Å). The sections collected in a water trough were transferred onto 200 mesh Cu−holey carbon grids (SPI Supplies, Structure Probe, Inc.) for analysis. For small-angle neutron scattering (SANS) measurements, the films were mounted on the back of cadmium sample holders with circular ~1 cm^2 apertures exposed to the neutron beam. SANS spectra were measured on the 30 m instrument NG-7 at the NIST Center for Neutron Research (NCNR), Gaithersburg, MD. The *Q*-range used was 0.004−0.517 Å^{-1}. The incident neutron wavelength was $\lambda = 6$ Å, with a wavelength resolution of $\Delta\lambda/\lambda = 0.11$. The measured data were reduced by application of a detector efficiency correction, an absolute scaling factor, and circular averaging of the scattered intensity.[25] The film thicknesses (required to compute the absolute scaling factors and permeability) were measured with a screw gauge. Dynamic mechanical thermal analysis (DMTA) measurements were carried out using a Rheometric Scientific Mark IV. Experimental runs were performed on film samples having a length of 20 mm, a width of 6 mm, and a thickness of 0.06 mm. A strain of 0.01% and a constant force of 0.015 N were applied to the samples with a heating rate of 3 °C/min in air.

Results and Discussion

Structural Analysis. Figure 2 shows the X-ray diffraction patterns of the as-synthesized layered AlPO, swollen layered AlPO, polymer, and PSF nanocomposite film. Ion-exchanging the ethylamine with $CTMA^+Cl^-$ leads to the expansion of the interlayer spacing, as observed in the shift of the (001) basal reflection to lower angle. Figure 3 presents a comparison of the ^{27}Al and ^{31}P solid-state MAS NMR spectra from the swollen AlPO with those of the as-made one. There is no substantial change in the coordination environment of Al and P after intercalation of the surfactant, indicating that the layer structure is preserved. For the 10 wt % PSF nanocomposite film, there is a broad peak at low angle in the XRD pattern as shown in Figure 2d. This low-angle peak centered at about 35 Å does not correspond to the basal spacing of the swollen layered AlPO nor to any reflection from the pure polyimide, demonstrating that the swollen layered AlPOs are intercalated with the polyimide. In addition, this peak is considerably broader (~25−60 Å) than the (001) reflection of the swollen layered AlPO, indicating a smaller inorganic domain size and/or a wider distribution of the interlayer spacings. By attributing the entire (minus instrumental) breadth of the low-angle peak to size broadening, one can make an approximate estimation of the average domain size of the intercalated layered AlPO using the Debye−Scherrer formula.[26] The average domain size estimated by this procedure is about 5−10 nm. This indicates that the intercalation of polymer leads to the delamination of the layers at least to nanosized domains (3−5 AlPO layers per domain).

The above estimate is further supported by transmission electron microscopy (TEM) imaging. Figure 4 shows

(25) http://www.ncnr.nist.gov/programs/sans/manuals/data_red.html, 2002.

(26) Krawitz, A. D. *Introduction to Diffraction in Materials Science and Engineering*; John Wiley & Sons: New York, 2001.

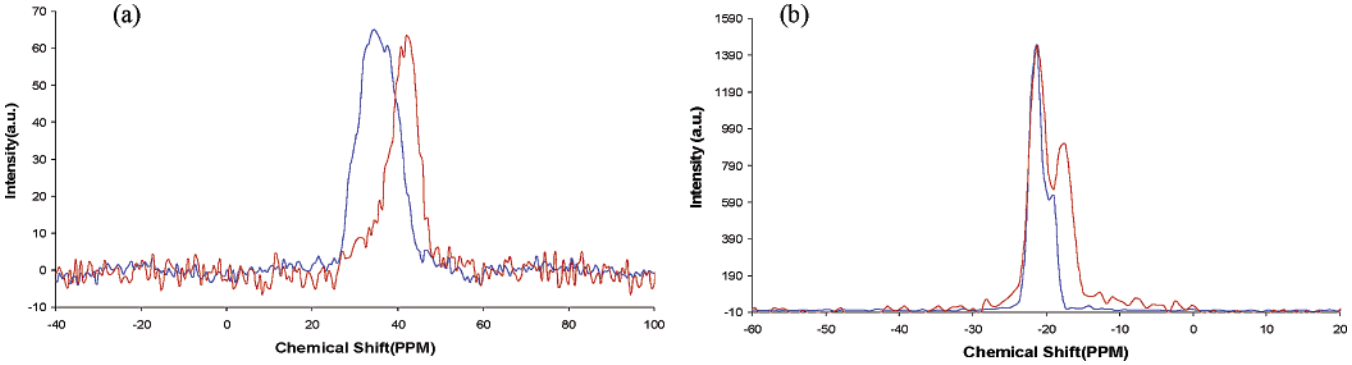

Figure 3. (a) ^{27}Al solid-state MAS NMR spectra (in reference to 0.1 M aqueous $Al_2(NO_3)_3$) and (b) ^{31}P solid-state MAS NMR spectra (in reference to 85 wt % H_3PO_4): blue line, as synthesized layered AlPO; red line, swollen layered AlPO.

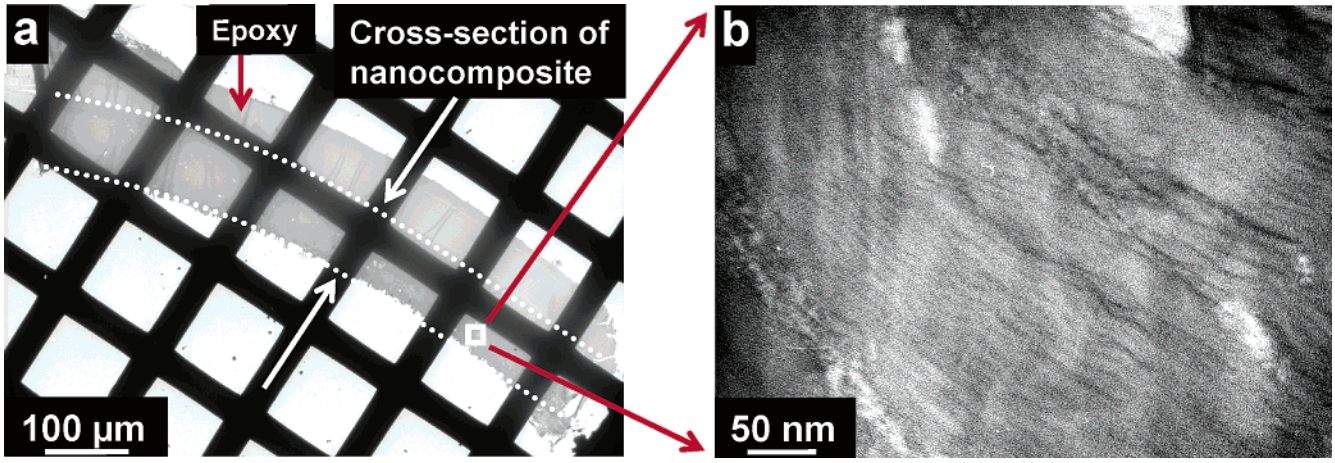

Figure 4. TEM images of the 10 wt % PSF nanocomposite membrane: (a) image showing a cross-section of the nanocomposite embedded in epoxy and (b) region marked in (a) revealing intercalated layers.

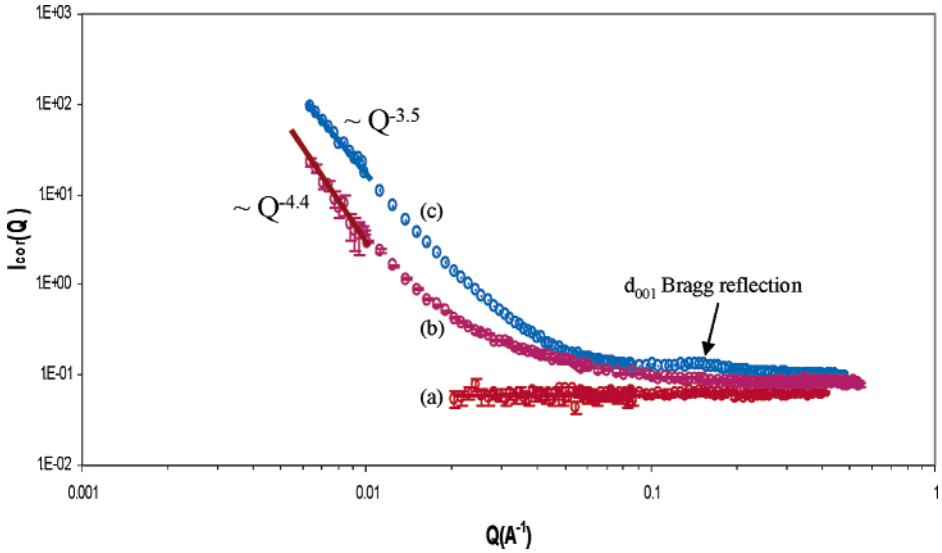

Figure 5. SANS spectra of (a) pure polyimide, (b) a polyimide/10 wt % as-synthesized AlPO composite, and (c) a 10 wt % PSF nanocomposite (neutron wavelength 6 Å).

TEM images of the 10 wt % PSF nanocomposite membrane. The dark contrast in the images corresponds to AlPO domains. They appear to be 5−10 nm thick, in agreement with the XRD estimate, and irregularly spaced at interdomain distances larger than 10 nm. Although the TEM images shown in Figure 4 suggest that at least some of the layers of AlPO are oriented in the desirable manner, i.e., perpendicular to the membrane cross-section, we also found evidence of such layers oriented parallel to the cross-section, suggesting that there is room for improvement of the layer orientation.

Figure 5 presents SANS spectra of the pure polyimide, polyimide/10 wt % as-synthesized AlPO composite film, and 10 wt % PSF nanocomposite film. Although the polymer/as-synthesized AlPO composite film contains as-synthesized crystals, no Bragg peaks are observed since the layer *d* spacing of the AlPO (~0.8 nm) falls

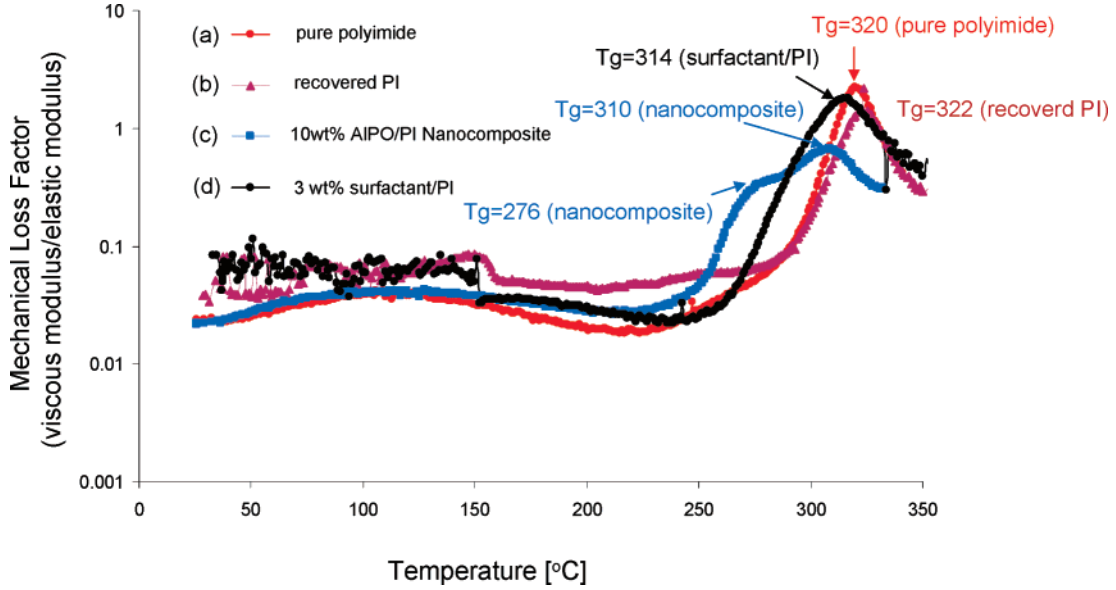

Figure 6. Mechanical loss factors of (a) pure polyimide (PI), (b) recovered PI from a 10 wt % PSF nanocomposite, (c) 10 wt % PSF nanocomposite, and (d) 3 wt % surfactant/PI composite.

outside the instrument range. In the low-Q region (<0.01 nm^{-1}), the as-synthesized AlPO composite film displays a $\sim Q^{-4.4}$ dependence consistent with the fact that the composite film contains large ($\sim 50\ \mu$m) crystals of $\sim 10^4$ layers each. The 10 wt % PSF nanocomposite film shows a Bragg peak at ~ 0.15 nm^{-1}, corresponding to the expanded d spacing (~ 4 nm) of the intercalated layers. This agrees well with the X-ray diffraction and TEM evidence described above. In the low-Q region (<0.01 nm^{-1}), the nanocomposite sample displays somewhat weaker power-law Q dependence (as compared to the composite sample) but is still consistent with a nanostructure of isolated few-layer particles separated by $\sim 10-100$ nm. No evidence for the exfoliation of single layers was observed since single exfoliated layers will show a much weaker dependence, $\sim Q^{-2}$, and no Bragg peak.[27−31]

Figure 6 shows the mechanical loss factors (defined as the ratio of the viscous modulus and elastic modulus) of the film samples. A recovered polyimide was obtained by centrifuging and removing the AlPO from the nanocomposite. The pure polyimide and the recovered polyimide show almost the same glass transition temperature at about 320 °C, indicating no structural change in the polymer phase upon the addition of the AlPO phase. In contrast, the 10 wt % PSF nanocomposite film has two distinctive broader peaks corresponding to two different glass transition temperatures (approximately 310 and 276 °C, respectively), indicating the presence of two different environments for the polymer. We assign these two different environments to the bulk phase and to the confined phase between the AlPO layers. The $T_g = 310$ °C (which is slightly lower than that of pure polyimide) is attributed to the presence of surfactant (about 3 wt %) in the bulk polymer phase in the nanocomposite. This is supported by a similar lower shift of T_g and peak broadening observed for the polyimide with 3 wt % surfactant as shown in Figure 6d. It appears that the presence of surfactant generates more free volume for the polymer chain, consequently making the relaxation of the polymer chain easier, leading to the decrease of the glass transition temperature. The lower T_g of 276 °C (significantly lower than that of the pure polyimide) can be attributed to the nanoconfinement of the polymer chain between the AlPO layers.[32]

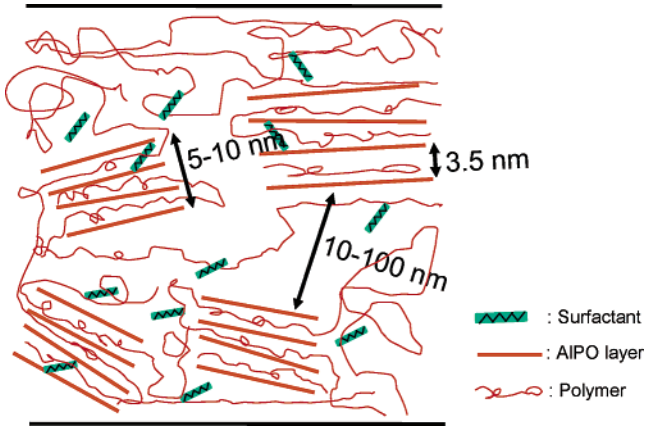

Figure 7. Schematic of the microstructure of the PSF nanocomposite.

Figure 7 summarizes our understanding of the microstructure of the nanocomposite membrane based on the microstructural characterization described above. The layered AlPO is delaminated to domains of nanometer thickness containing three or four layers with an interlayer spacing of 3.5 nm. These inorganic domains are randomly oriented with interdomain spacing of 10−100 nm. The polymer chains penetrate into the interlayer space, and some of the surfactant molecules reside in the bulk polymer phase. There is no evidence for the

(27) Hanley, H. J. M.; Straty, G. C.; Tsvetkov, F. *Langmuir* **1994**, *10*, 3362−3364.
(28) Hanley, H. J. M.; Muzny, C. D.; Ho, D. L.; Glinka, C. J.; Manias, E. *Int. J. Thermophys.* **2001**, *22*, 1435−1448.
(29) Avery, R. G.; Ramsay, J. D. F. *J. Colloid Interface Sci.* **1986**, *109*, 448−454.
(30) Ho, D. L.; Briber, R. M.; Glinka, C. J. *Chem. Mater.* **2001**, *13*, 1923−1931.
(31) Shang, C.; Rice, J. A. *Phys. Rev. E* **2001**, *6402*.
(32) Ellison, C. J.; Torkelson, J. M. *Nat. Mater.* **2003**, *2*, 695−700.

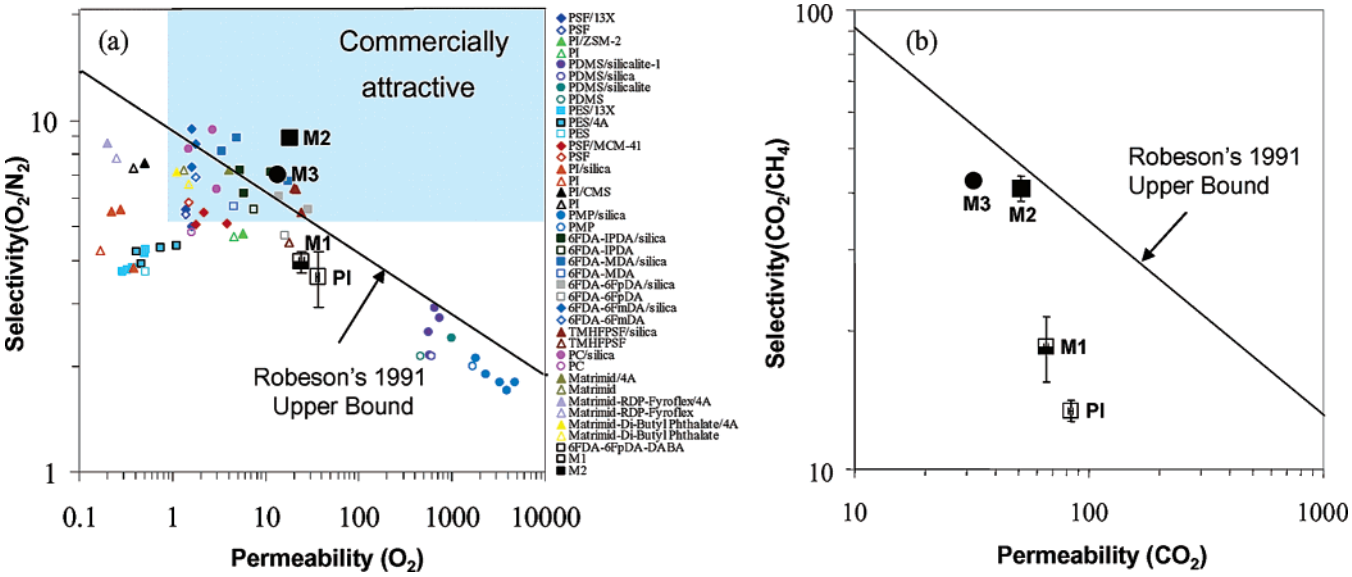

Figure 8. Nanocomposite membrane performance: (a) oxygen/nitrogen selectivity as a function of oxygen permeability in contrast to those of various polymer and mixed-matrix membranes in the literature[2−4,6,7,10,44−49] and (b) carbon dioxide/methane selectivity as a function of carbon dioxide permeability. Key: □, pure polyimide, ⬓, M1; ■, M2; ●, M3. M1 (nanocomposite membrane 1): 5 wt % AlPO and 95 wt % polyimide stirred in THF at 30 °C for 4 days. M2 (nanocomposite membrane 2): 10 wt % AlPO and 90 wt % polyimide stirred in THF at 30 °C for 4 days. M3 (nanocomposite membrane 3): 10 wt % swollen AlPO and 90 wt % polyimide stirred in THF at 30 °C for 4 days and heated at about 60 °C for 6 h before casting. The commercially attractive region was identified by Koros and co-workers.[2]

Table 1. PSF Nanocomposite Membrane Permeability[a]

	kinetic diameter (Å)	Pauling length/width (Å)	permeability[b] polymer[c]	M1	M2	M3
He	2.6	~3	178	148	94.4	67.5
CO_2	3.3	5.1/3.7	84	66	51	28.3
O_2	3.46	3.9/2.8	36	24	18.5	9.3
N_2	3.64	4.1/3.0	10	6.2	2.1	1.2
CH_4	3.8	4.2	6	3.6	1.3	0.7

[a] Measurement recorded at 30 °C. M1 (nanocomposite membrane 1): 5 wt % swollen AlPO and 95 wt % polyimide stirred in THF at 30 °C for 4 days. M2 (nanocomposite membrane 2): 10 wt % swollen AlPO and 90 wt % polyimide stirred in THF at 30 °C for 4 days. M3 (nanocomposite membrane 3): 10 wt % swollen AlPO and 90 wt % polyimide stirred in THF at 30 °C for 4 days and heated at about 60 °C for 6 h before casting. [b] Permeability in Barrer: 1 Barrer = 10^{-10} (cm^3 (STP)·cm)/(cm^2·s·cmHg). [c] 56100 MW 6FDA−6FpDA-8%−DABA.

Table 2. PSF Nanocomposite Membrane Selectivity

selectivity	PI	M1	M2	M3
$He-O_2$	4.93	6.07	8.91	7.26
$He-N_2$	17.69	23.99	45.40	56.25
$He-CH_4$	28.66	41.56	75.54	96.89
$He-CO_2$	1.55	2.25	1.85	2.39
O_2-N_2	3.59	3.95	8.91	7.75
O_2-CH_4	5.81	6.85	14.82	13.35
N_2-CH_4	1.62	1.73	1.66	1.72
CO_2-O_2	2.31	2.70	2.76	3.04
CO_2-N_2	8.28	10.68	24.60	23.58
CO_2-CH_4	13.42	18.50	40.93	40.62

exfoliation of the layers into single layers and for the desired alignment of the layers perpendicular to the thickness of the membrane. There is, therefore, still a need for further processing improvements to obtain a fully exfoliated highly oriented nanocomposite.

Single-Gas Permeation. Tables 1 and 2 compare the permeability and selectivity for various gases of a pure polyimide membrane with those of a 5 wt % and a 10 wt % PSF nanocomposite membrane. The higher the percentage of the AlPO flakes, the more pronounced the decrease in permeability. The permeability decrease is attributed to the large aspect ratio of the AlPO flakes increasing the tortuosity of the transport path of the gas molecules.[14,17,18] The permeability reduction is more pronounced as the size of the penetrating gas molecule increases. Consequently, the presence of the AlPO flakes also leads to significant selectivity improvement. Figure 8 presents oxygen/nitrogen selectivity as a function of oxygen permeability (a) and carbon dioxide/methane selectivity as a function of carbon dioxide permeability (b). The solid lines indicate Robeson's 1991 upper bound for the performance of polymeric membrane materials.[33] As seen in Figure 8, the combination of oxygen/nitrogen selectivity and oxygen permeability of the 10 wt % PSF nanocomposite membrane lies well beyond the upper bound, falling in the commercially attractive region,[2] while carbon dioxide/methane selectivity and carbon dioxide permeability approach the upper bound. It should be pointed out that this significant improvement of the membrane performance is a result of only 10 wt % (or possibly less considering the misoriented fraction of flakes) of the layered AlPO.[18] To achieve similar improvements with mixed-matrix membranes that contain typically isotropic molecular sieve particles, a considerably larger amount of the selective phase would be required.[2,3] Further optimization can be achieved by complete exfoliation of the AlPO layers, and by orientation of the layers only parallel to the membrane surface. Furthermore, use of layered materials with different transport properties may provide the means for further selectivity and permeability improvement. Such materials include the recently reported layered silicate AMH-3[34] and several other existing layered AlPOs.[35−41]

(33) Robeson, L. M. *J. Membr. Sci.* **1991**, *62*, 165−185.
(34) Jeong, H. K.; Nair, S.; Vogt, T.; Dickinson, L. C.; Tsapatsis, M. *Nat. Mater.* **2003**, *2*, 53−58.
(35) Vidal, L.; Gramlich, V.; Patarin, J.; Gabelica, Z. *Chem. Lett.* **1999**, 201−202.
(36) Wei, B.; Yu, J. H.; Shi, Z.; Qiu, S. L.; Li, J. Y. *J. Chem. Soc., Dalton Trans.* **2000**, 1979−1980.

Table 3. Calculated Effective AlPO Particle Aspect Ratio (α) and Calculated Effective Permeabilities[a] of He, CO_2, O_2, and N_2

	M1	M2	M3	av
α	19.4	26.3	84.5	
P_{He}	25.1	15.7	10.0	16.9 ± 7.6
P_{CO_2}	8.6	10.3	3.9	7.6 ± 3.3
P_{O_2}	1.5	2.9	1.7	1.9 ± 0.9
P_{N_2}	0.2	0.1	0.1	0.2 ± 0.05
P_{CH_4}	0.07	0.07	0.07	0.07

[a] Permeability in Barrer.

Finally, the properties of the polymer are also important in the success of the selective-flake applications[11] and further optimization can be achieved by proper polymer/flake property matching.

Role of the Layered AlPO. The permeability of the AlPO flakes is not known. However, by assuming a permeability of methane (which has the largest kinetic diameter) through the AlPO flake, one can estimate the effective aspect ratio of the flake using a semiempirical effective medium model developed by Cussler[11] which in turn allows the permeabilities of other gas molecules through the AlPO flakes to be estimated. Table 3 shows calculations based on the model to describe transport through composites containing oriented selective flakes. First, we calculate an effective aspect ratio, α, for the layers (flakes) using eq 1, by assuming a small permeability of CH_4 through the flake (in this case, 0.07 Barrer).

$$\frac{P_{\text{polymer}}}{P_{\text{membrane}}} = 1 - \phi + \left[\frac{1}{\delta\phi} + \frac{1-\phi}{\alpha^2\phi^2}\right]^{-1} \qquad (1)$$

The calculated aspect ratio, α, is smaller than the actual one (at least 50 as estimated by TEM), reflecting in part the absence of a preferred orientation of the AlPO layers in our nanocomposites and suggesting that there is room for improving selectivity or reducing the amount of AlPO layers if a preferred orientation is achieved. The effective permeabilities for various gases in AlPO, P_{gas}, were then calculated for each gas by finding $\delta = P_{polymer}/P_{gas}$ from the above equation.

Unlike composites containing large (>100 nm) molecular sieve particles, the effective permeabilities cannot be interpreted as a result of intracrystalline adsorption and transport, because interfacial and surface effects are probably playing a major role in determining the transport properties of the nanocomposite. Moreover, the calculated values of effective permeability incorporate a scaling factor for an effective ϕ that is smaller than the actual ϕ due to the lack of a preferred orientation. Finally, these values would have changed, had we used another permeability for CH_4. However, despite the above-mentioned limitations of this preliminary analysis, the relative magnitudes of the calculated effective permeabilities clearly indicate that the AlPO layers act as molecular sieves, favoring the gases with smaller molecular dimensions. Despite the scatter, the results are consistent for all three membranes.

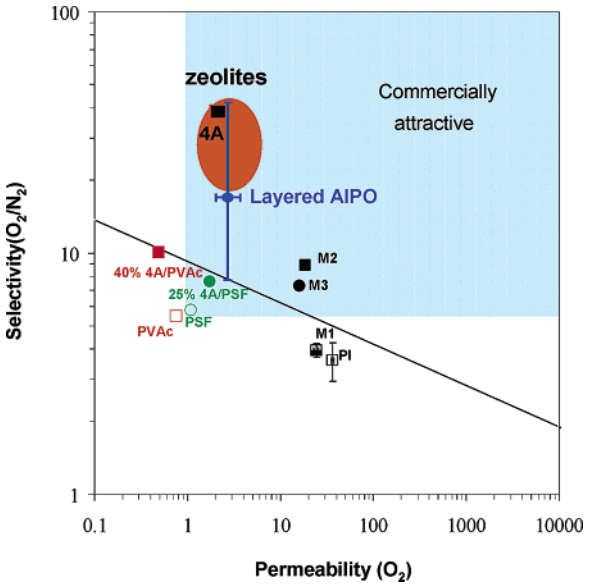

Figure 9. Estimated oxygen permeability and selectivity for oxygen over nitrogen of layered AlPO (see the text for details) using the model of ref 11. The corresponding experimentally determined properties of the nanocomposites marked PI (pure polyimide), M1 (5% AlPO), M2, and M3 (10% AlPO) from Figure 8 are also provided. For comparison, polyvinyl acetate (PVAc) and zeolite 4A/PVAc (40% zeolite A) mixed-matrix membrane data are included from ref 42 and polysulfone (PSF) and zeolite 4A/PSF (25% nanocrystalline zeolite A) data from ref 43.

Figure 9 shows the estimated oxgyen permeability and selectivity over nitrogen of the layered AlPO in the Robeson plot. The estimated performance of the layered AlPO is comparable to those of zeolites. It is also illustrated that while mixed-matrix membranes with zeolite 4A require a large amount of the selective phase (25−40%) to achieve appreciable improvement,[42,43] only 10 wt % of the selective phase in PSF nanocomposite membranes enhances membrane performance substantially.

Conclusions

The first polymer/selective-flake nanocomposite membranes have been fabricated with a polyimide and a porous layered aluminophosphate. These membranes show substantially improved selectivities of oxygen over nitrogen and carbon dioxide over methane with only 10 wt % of the AlPO layers. This enhancement in mem-

(37) Yu, J. H.; Xu, R. R. *Acc. Chem. Res.* **2003**, *36*, 481−490.
(38) Oliver, S.; Kuperman, A.; Lough, A.; Ozin, G. A. *Inorg. Chem.* **1996**, *35*, 6373−6380.
(39) Yao, Y. W.; Natarajan, S.; Chen, J. S.; Pang, W. Q. *J. Solid State Chem.* **1999**, *146*, 458−463.
(40) Yuan, H. M.; Zhu, G. S.; Chen, J. S.; Chen, W.; Yang, G. D.; Xu, R. R. *J. Solid State Chem.* **2000**, *151*, 145−149.
(41) Tuel, A.; Gramlich, V.; Baerlocher, C. *Microporous Mesoporous Mater.* **2002**, *56*, 119−130.
(42) Mahajan, R.; Burns, R.; Schaeffer, M.; Koros, W. J. *J. Appl. Polym. Sci.* **2002**, *86*, 881−890.
(43) Wang, H. T.; Holmberg, B. A.; Yan, Y. S. *J. Mater. Chem.* **2002**, *12*, 3640−3643.
(44) Pinnau, I.; He, Z. U.S. Patent 6,316,684, 2001.
(45) Koros, W. J.; Vu, D. Q.; Mahajan, R.; Miller, S. J. U.S. Patent 6,503,295, 2003.
(46) Joly, C.; Smaihi, M.; Porcar, L.; Noble, R. D. *Chem. Mater.* **1999**, *11*, 2331−2338.
(47) Moaddeb, M.; Koros, W. J. *J. Membr. Sci.* **1997**, *125*, 143−163.
(48) Reid, B. D.; Ruiz-Trevino, A.; Musselman, I. H.; Balkus, K. J.; Ferraris, J. P. *Chem. Mater.* **2001**, *13*, 2366−2373.
(49) Suer, M. G.; Bac, N.; Yilmaz, L. *J. Membr. Sci.* **1994**, *91*, 77−86.

brane performance is attributed to the molecular sieving property of the AlPO layers of high aspect ratio. The improved selective properties of the first PSF nanocomposite reported here open the possibility for extending this concept to other separations using nanocomposite materials consisting of a continuous phase of an easily processed soft material and a dispersed flakelike molecular sieve.

Acknowledgment. We acknowledge support from the NSF (Grants CTS-0107488 and CTS-0091406). We are grateful of Dr. L. C. Dickinson (University of Massachusetts) and Dr. Man-Ho Kim (NIST) for their help in collecting NMR and SANS spectra, respectively. We are also grateful to M. Woo for her help in preparing Figure 8a.

CM049154U